

32 collisions. These excesses may originate from coherent photon-induced in-
 33 teractions. Measurements of dilepton and J/ψ production at very low p_T
 34 for different collision energies, collision species, and centralities can shed
 35 new light on the origin of the excess [10, 11].

36 In these proceeding, we present invariant mass distributions of low- p_T
 37 e^+e^- and $\mu^+\mu^-$ pairs production. The energy dependence of $\sqrt{\langle p_T^2 \rangle}$
 38 for e^+e^- pairs and low- p_T J/ψ excess yields are also shown. Theoretical
 39 predictions are compared with data.

40 2. Experiment and Analysis

41 The data reported are collected with the STAR detector. The 200 and
 42 54.4 GeV Au+Au collision data taken in 2011 and 2017 respectively are used
 43 for the dielectron analysis. The dataset that the dimuon analysis uses is the
 44 200 GeV Au+Au collision data taken in 2014. J/ψ analysis uses Zr+Zr and
 45 Ru+Ru collisions at 200 GeV recorded in 2018. The main sub-detectors
 46 used are the Time Projection Chamber (TPC) [12] and the Time of Flight
 47 (TOF) [13]. The TPC is the main detector for charged-particle tracking,
 48 and it can also measure the ionization energy loss to provide charged-particle
 49 identification. The TOF is used to identify particles by measuring the flight
 50 time. By combining the TPC and TOF, electrons and muons can be iden-
 51 tified with high purity. The like-sign distribution is used to estimate the
 52 combinatorial and correlated background, with the mixed-event technique
 53 used to correct the acceptance difference. After subtracting background
 54 from the unlike-sign distribution, the raw signal can be obtained, which
 55 is then corrected for detector effects. Finally, a Monte-Carlo simulation is
 56 applied to evaluate the hadronic cocktail contribution.

57 3. Results and Discussion

58 3.1. Low- p_T e^+e^- pair production in Au+Au collisions

59 After statistically subtracting the hadronic cocktail contribution from
 60 the inclusive e^+e^- pairs, the invariant mass distributions of excess pairs
 61 for $p_T < 0.15$ GeV/c are shown in Fig. 1 for $\sqrt{s_{NN}} = 54.4$ GeV and
 62 $\sqrt{s_{NN}} = 200$ GeV in different centralities. The invariant mass spectra
 63 are smooth and featureless even in the range of known vector mesons. This
 64 is a consequence of the quantum numbers of the two photons involved in the
 65 Breit-Wheeler process where the helicity state $J_z = 0$ is absent for real pho-
 66 tons but necessary for exclusive vector-meson production. These excesses
 67 are also consistent with the lowest order EPA-QED predictions [15, 16]
 68 for the collision of linearly polarized photons quantized from the extremely

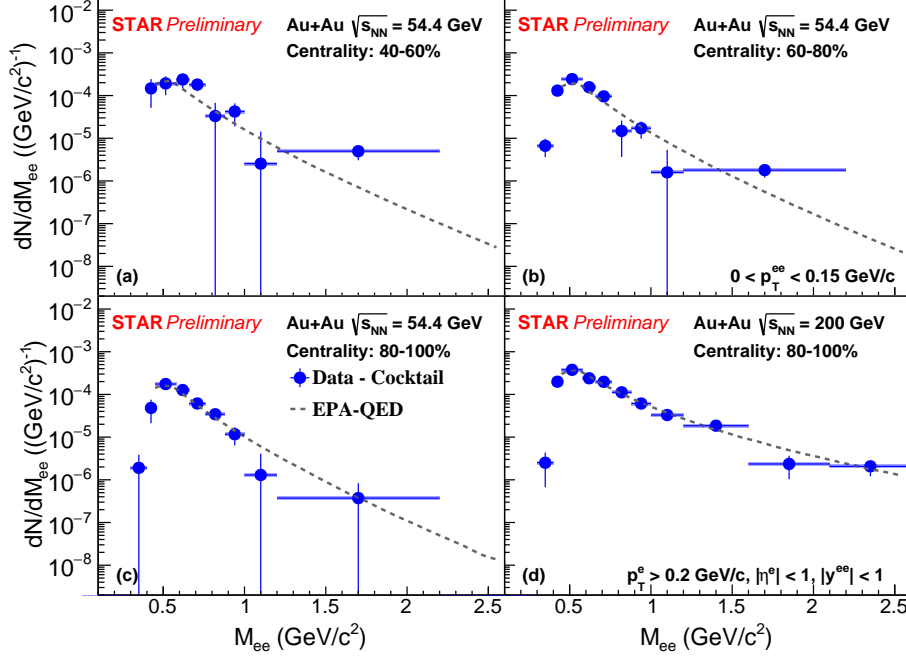


Fig. 1. (color online) The low- p_T ($p_T < 0.15$ GeV/c) e^+e^- excess mass spectra (Data – Cocktail) within the STAR acceptance in Au+Au collisions at $\sqrt{s_{NN}} = 54.4$ GeV in the centrality of (a) 40-60%, (b) 60-80%, (c) 80-100% and (d) $\sqrt{s_{NN}} = 200$ GeV in the centrality of 80-100% compared to the lowest order EPA-QED predictions (dashed line). Statistical uncertainties are shown as vertical bars on all points, while systematic uncertainties are shown as blue boxes which are smaller than the marker size.

69 strong electromagnetic fields generated by the highly charged Au nuclei at
70 ultra-relativistic speed.

71 Since $\sqrt{\langle p_T^2 \rangle}$ is sensitive to p_T broadening, we study $\sqrt{\langle p_T^2 \rangle}$ for
72 e^+e^- pairs as a function of beam energy in different centralities shown in
73 Fig. 2. $\sqrt{\langle p_T^2 \rangle}$ decreases with increasing impact parameter at both 54.4
74 and 200 GeV. For high precision results at $\sqrt{s_{NN}} = 200$ GeV in UPCs, the
75 consistency between the EPA-QED prediction [15, 16] and our measurement
76 shows that the EPA-QED predictions at $\sqrt{s_{NN}} = 200$ GeV can be treated
77 as a baseline. 3.7σ difference is found when comparing all the data points
78 at $\sqrt{s_{NN}} = 54.4$ GeV to EPA-QED predictions at $\sqrt{s_{NN}} = 200$ GeV,
79 which arises from the energy dependence of $\sqrt{\langle p_T^2 \rangle}$ and possible final
80 state effects. e^+e^- pairs produced from photon-photon interactions are

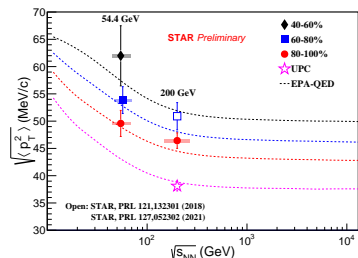


Fig. 2. (color online) The energy dependence of $\sqrt{\langle p_T^2 \rangle}$ for e^+e^- pairs compared to the lowest order EPA-QED predictions shown as dashed line in Au+Au collisions for the centrality intervals of 40-60%, 60-80%, 80-100%, and UPCs. Statistical uncertainties are shown as vertical bars, while systematic uncertainties are shown as boxes. Open markers are extracted from Ref. [7, 14].

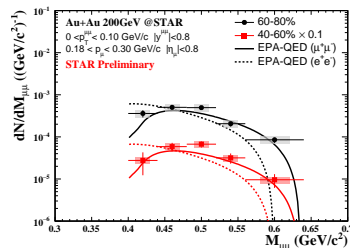


Fig. 3. (color online) The low- p_T ($p_T < 0.1$ GeV/c) $\mu^+\mu^-$ excess mass spectra (Data - Cocktail) in Au+Au collisions at $\sqrt{s_{NN}} = 200$ GeV for the centrality intervals of 40-60% and 60-80% compared to the lowest order EPA-QED predictions. Statistical uncertainties are shown as vertical bars, while systematic uncertainties are shown as boxes.

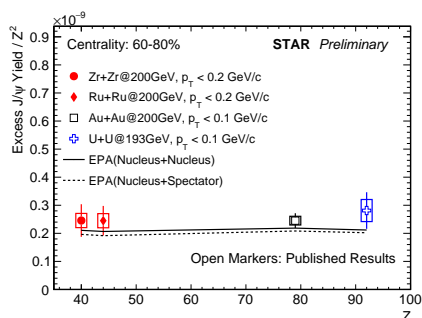


Fig. 4. (color online) Low p_T J/ψ excess yields scaled with Z^2 as a function of Z compared to model predictions in Zr+Zr, Ru+Ru, Au+Au and U+U collisions for the centrality interval of 60-80%. Statistical uncertainties are shown as vertical bars, while systematic uncertainties are shown as boxes. Open markers are extracted from Ref. [9].

81 mostly back to back, and final state effects due to trapped magnetic field or
82 Coulomb scattering in the QGP can lead to the observed p_T broadening.

83 3.2. Low- p_T $\mu^+\mu^-$ pair production in Au+Au collisions

84 After statistically subtracting the hadronic cocktail contribution from
85 the inclusive $\mu^+\mu^-$ pairs, the invariant mass distributions of excess pairs
86 for $p_T < 0.1$ GeV/c are shown in Fig. 3 for $\sqrt{s_{NN}} = 200$ GeV in different
87 centralities. For real photon interactions, EPA-QED [15, 16] predicts differ-
88 ent pair mass distributions for dimuon and dielectron production due to
89 the mass difference, which are shown as solid and dotted lines, respectively.

90 Our data are well described by EPA-QED predictions based on real photon
91 interactions to dimuon.

92 predicts different pair mass distributions for dimuon and dielectron
93 production due to the mass difference, which are shown as solid and dotted
94 lines, respectively.

95 3.3. Low- p_T J/ψ production in $Zr+Zr$ and $Ru+Ru$ collisions

96 Figure 4 shows low p_T J/ψ excess yields scaled with Z^2 (Z : nucleus
97 charge number) as a function of Z . A flat distribution is seen, which reveals
98 that the J/ψ excess yield is proportional to Z^2 and not sensitive to the
99 details of the nuclear form factor or the impact parameter. Our data can
100 be described by EPA predictions [17].

101 4. Summary

102 We report the measurements of low- p_T e^+e^- and $\mu^+\mu^-$ pairs produc-
103 tion in noncentral Au+Au collisions at $\sqrt{s_{NN}} = 54.4$ GeV and $\sqrt{s_{NN}} =$
104 200 GeV. The observed excesses can be well described by EPA-QED pre-
105 dictions for both channels. There is a 3.7σ difference in $\sqrt{\langle p_T^2 \rangle}$ of e^+e^-
106 pairs between the measurement at $\sqrt{s_{NN}} = 54.4$ GeV and EPA-QED pre-
107 dictions at $\sqrt{s_{NN}} = 200$ GeV, indicating collision energy dependence and
108 possible final state effects. The low- p_T J/ψ production in isobaric collisions
109 ($^{96}_{44}Ru + ^{96}_{44}Ru, ^{96}_{40}Zr + ^{96}_{40}Zr$) at $\sqrt{s_{NN}} = 200$ GeV is also measured. J/ψ
110 excess yields scaled with Z^2 is flat against Z , which reveals that photopro-
111 duced J/ψ yields are proportional to Z^2 but not sensitive to the details of
112 the nuclear form factor or the impact parameter.

113 5. Acknowledgements

114 This work was presented for the STAR Collaboration and partially
115 funded by the National Natural Science Foundation of China under Grant
116 No. 12075139.

REFERENCES

- 117 [1] Miklos Gyulassy and Larry McLerran. New forms of QCD matter discovered
118 at RHIC. *Nucl. Phys. A*, 750:30–63, 2005.
- 119 [2] John Adams et al. Experimental and theoretical challenges in the search for
120 the quark gluon plasma: The STAR Collaboration’s critical assessment of the
121 evidence from RHIC collisions. *Nucl. Phys. A*, 757:102–183, 2005.

- 122 [3] F. Krauss, M. Greiner, and G. Soff. Photon and gluon induced processes in
123 relativistic heavy ion collisions. *Prog. Part. Nucl. Phys.*, 39:503–564, 1997.
- 124 [4] Leonid Frankfurt, Werner Koepf, and Mark Strikman. Diffractive heavy
125 quarkonium photoproduction and electroproduction in QCD. *Phys. Rev. D*,
126 57:512–526, 1998.
- 127 [5] J. Adams et al. Production of e^+e^- pairs accompanied by nuclear dissociation
128 in ultra-peripheral heavy ion collision. *Phys. Rev. C*, 70:031902, 2004.
- 129 [6] Betty Abelev et al. Coherent J/ψ photoproduction in ultra-peripheral Pb-Pb
130 collisions at $\sqrt{s_{NN}} = 2.76$ TeV. *Phys. Lett. B*, 718:1273–1283, 2013.
- 131 [7] Jaroslav Adam et al. Low- p_T e^+e^- pair production in Au+Au collisions at
132 $\sqrt{s_{NN}} = 200$ GeV and U+U collisions at $\sqrt{s_{NN}} = 193$ GeV at STAR. *Phys.*
133 *Rev. Lett.*, 121(13):132301, 2018.
- 134 [8] Jian Zhou. Low- p_T $\mu^+\mu^-$ pair production in Au+Au collisions at $\sqrt{s_{NN}} =$
135 200 GeV at STAR. *EPJ Web Conf.*, 259:13014, 2022.
- 136 [9] J. Adam et al. Observation of excess J/ψ yield at very low transverse momenta
137 in Au+Au collisions at $\sqrt{s_{NN}} = 200$ GeV and U+U collisions at $\sqrt{s_{NN}} = 193$
138 GeV. *Phys. Rev. Lett.*, 123(13):132302, 2019.
- 139 [10] Xiaofeng Wang, James Daniel Brandenburg, Lijuan Ruan, Fenglan Shao,
140 Zhangbu Xu, Chi Yang, and Wangmei Zha. Energy Dependence of the Breit-
141 Wheeler process in Heavy-Ion Collisions and its Application to Nuclear Charge
142 Radius Measurements. 7 2022.
- 143 [11] James Daniel Brandenburg, Zhangbu Xu, Wangmei Zha, Cheng Zhang, Jian
144 Zhou, and Yajin Zhou. Exploring gluon tomography with polarization depend-
145 ent diffractive J/ψ production. 7 2022.
- 146 [12] M. Anderson et al. The Star time projection chamber: A Unique tool for
147 studying high multiplicity events at RHIC. *Nucl. Instrum. Meth. A*, 499:659–
148 678, 2003.
- 149 [13] W. J. Llope. Multigap RPCs in the STAR experiment at RHIC. *Nucl. Instrum.*
150 *Meth. A*, 661:S110–S113, 2012.
- 151 [14] Jaroslav Adam et al. Measurement of e^+e^- Momentum and Angular Dis-
152 tributions from Linearly Polarized Photon Collisions. *Phys. Rev. Lett.*,
153 127(5):052302, 2021.
- 154 [15] Wangmei Zha, James Daniel Brandenburg, Zebo Tang, and Zhangbu Xu. Ini-
155 tial transverse-momentum broadening of Breit-Wheeler process in relativistic
156 heavy-ion collisions. *Phys. Lett. B*, 800:135089, 2020.
- 157 [16] James Daniel Brandenburg, Wangmei Zha, and Zhangbu Xu. Mapping the
158 electromagnetic fields of heavy-ion collisions with the Breit-Wheeler process.
159 *Eur. Phys. J. A*, 57(10):299, 2021.
- 160 [17] W. Zha, L. Ruan, Z. Tang, Z. Xu, and S. Yang. Coherent photo-produced J/ψ
161 and dielectron yields in isobaric collisions. *Phys. Lett. B*, 789:238–242, 2019.